Stimuli-responsive photoluminescent and structural properties of MIL-53(Al) MOF for sensing applications

OPEN ACCESS
IOP Publishing
Journal of Physics: Condensed Matter
J. Phys.: Condens. Matter **36** (2024) 315401 (9pp)
https://doi.org/10.1088/1361-648X/ad43a4

Stimuli-responsive photoluminescent and structural properties of MIL-53(Al) MOF for sensing applications

T Ul Rehman*, S Agnello, F M Gelardi, M M Calvino, G Buscarino and M Cannas

Dipartimento di Fisica e Chimica–Emilio Segrè, Università degli Studi di Palermo, 90123 Palermo, Italy

E-mail: tanzeelul.rehman@unipa.it

Received 10 November 2023, revised 5 April 2024
Accepted for publication 25 April 2024
Published 9 May 2024

Abstract

Metal–organic frameworks (MOFs) are an intriguing group of porous materials due to their potential influence on the development of indispensable technologies like luminescent sensors and solid-state light devices, luminescent multifunctional nanomaterials. In this research work we explored MIL-53(Al), an exceptional class of MOF that, along with guest adsorption, undergoes structural transitions exhibiting breathing behavior between narrow pore and large pore under temperature and mechanical stress. Therefore, we opted for the time resolved luminescence and FT-Raman spectroscopy to investigate the mechanochromic and thermochromic response of this material under external stimuli. Intriguingly, when subjected to temperature changes, MIL-53(Al) exhibited a ratiometric fluorescence behavior related to the reversible relationship of photoluminescence emission intensity with respect to temperature. Moreover, under higher mechanical stress MIL-53(Al) displayed turn-on behavior in emission intensity, hence offering a thrilling avenue for the application in mechanically deformed-based luminescent sensors and ratiometric fluorescence temperature sensors.

Keywords: LMOFs, MIL-53(Al), time-resolved photoluminescence, mechanochromic, thermochromic

1. Introduction

Optoelectronics device light-emitting material research has never stopped intensifying and the recently found hybrid organic-inorganic materials have caused a tremendous change in this field [1, 2]. The ability of luminous nanoparticles to work as a non-invasive sensing device—for example, highly sensitive sensors of pollutants, volatile organic compounds, pH, pressure, or temperature—has attracted a lot of interest among these applications [3–6]. Metal-organic frameworks (MOFs) have gained significant promise across a variety of applications owing to their distinctive structural properties and tunable functionalities [7]. In fact, these highly porous materials boast extensive surface areas and tailor-made pore structures, making them ideal candidates for gas storage, separation, and sensing applications [8]. Moreover, MOFs exhibit exceptional catalytic activity, making them valuable in catalysis for chemical transformations and green synthesis processes [3, 8]; their tunable properties enable MOFs to be designed for energy storage systems, improving the efficiency of battery electrodes [9, 10]. As a result of ongoing research and development, MOFs continue to advance across a wide range of applications, offering innovative solutions to pressing societal and environmental challenges.

The development of numerous new examples of MOFs, whose chemical structure and physical properties can be modified to afford different applications such as lighting,

* Author to whom any correspondence should be addressed.

luminescent thermometry, and bio-imaging, has particularly boosted the field of luminescent MOFs, also known as LMOFs [11, 12], that may overcome the inherent limits of conventional systems [11, 13, 14]. Utilizing tunable LMOFs materials, for instance, can address drawbacks of commercially available thermometers such as fragility, slow response, lack of high precision, and high sensitivity subject to electric and magnetic fields [15, 16]. Then, the development of nano-sized LMOFs-based thermometers not only eliminates the previous restrictions but also opens a wide range of opportunities, such as for understanding heat transfer mechanisms occurring at living cells or in integrated electronic circuits; they provide a quick response time, operate without making a contact with the surface (non-invasive) and are unaffected by magnetic and electric fields [17–20].

For these purposes, a luminescent material with huge potential for multitasking detection capabilities is MIL-53(Al), that belongs to a prototypical family of flexible MOFs, whose structure is composed of corner-sharing MO4(OH)2 octahedra connected by 1,4-benzenedicarboxylic (BDC) acids. Different studies have demonstrated a remarkable photoluminescence (PL) of powder MIL-53(Al) under UV light excitation, with a spectrum consisting of two partially superimposed bands: the first peaking approximately at 400 nm is similar to that observed in aqueous solution; the second is peaked around 450 nm. Herein, we provide a thorough examination of the luminescence of solid-state MIL-53(Al), with an emphasis on identifying the electronic transitions that occur within the material, to uncover the correlations between luminescence properties (spectral and temporal decay) and structural changes caused by breathing from large pore (LP) to narrow pore (NP). Our goal is to investigate the luminescent response to different external stimuli, such as temperature and mechanical pressure, to assess its potential use as a non-invasive sensor.

2. Samples and methods

MIL-53(Al), utilized in this work, is in the form of a powder of commercial origin and purchased from Sigma-Aldrich (Basolite® A100). Two distinct series of samples were prepared from this material. The first series was achieved by activating the raw powder at 423 K in air for 12 h. The second series was prepared by pressing the raw powder into different pellets under a hydraulic press with a range up to 0.22 GPa. Additionally, a third powder sample was also considered, for comparison purposes, which was an organic linker of MIL-53(Al), named terephthalic acid (BDC, 99+%), provided by the Sigma-Aldrich as well.

Using a Rigaku Miniflex diffractometer equipped with a Cu Kα source (1.541 Å), powder x-ray diffraction (PXRD) was employed to analyze the crystalline structure of MIL-53(Al) MOF and free BDC linkers. We obtained diffraction data with a range of 2θ angles from 7° to 70° at a step size of 0.01° and a rate of 1° min^{-1}. By means of thermogravimetric analysis (TGA), we looked at the thermal stability of MIL-53(Al) and free BDC linkers as well. All the samples were heated in a platinum pan from ambient temperature to 800 °C at a scanning rate of 20 °C min^{-1} using a TGA 550 (Discovery Series—TA Instruments) used for the analysis.

Stimuli-responsive properties of MIL-53(Al) were investigated by using time-resolved PL spectroscopy, under a tunable laser excitation provided by an optical parametric oscillator (VIBRANT OPOTEK) pumped by the third harmonic (3.49 eV) of a Nd:YAG laser (pulse width 5 ns, repetition rate 10 Hz). The emitted light was analyzed by a monochromator equipped with a grating of 150 lines mm^{-1} and blaze wavelength 300 nm and acquired by an intensified CCD camera driven by a delay generator (PIMAX Princeton Instruments) setting the acquisition time window (T_W) and the delay time (T_D) with respect to the arrival of laser pulses [21]. All the emission spectra were detected with a bandwidth of 5 nm and corrected for the monochromator dispersion. The impact of mechanical pressure on the vibrational properties of MIL-53(Al) was examined by FT-Raman spectroscopy. FT-Raman spectra were detected by a Bruker Vertex 70 v RAMII spectrometer in the range of 0–3500 cm^{-1} using a Nd:YAG-Laser (1064 nm) excitation, with power of 500 mW, averaging 200 scans, the spectral resolution was kept at 3 cm^{-1}.

3. Results and discussion

3.1. Structural and thermal properties of MIL-53(Al) and free BDC linkers

As shown in figure 1(A), the PXRD data revealed that MIL-53(Al) has a monoclinic hydrated narrow pore (HyNP) structure with a space group of C 2/c, respectively. The following are the parameters of the unit cell: $a = 17.63$ Å, $b = 11.76$ Å, and $c = 4.55$ Å, and their corresponding angles are $\alpha = 90°$, $\beta = 104.2°$, and $\gamma = 90°$. The volume of the unit cell is determined to be 943.34 Å$^{\wedge 3}$. As compared to the free BDC linkers, the broadening of the PXRD peaks of MIL-53(Al) and the shifting in the peak's positions indicate that the organic linkers are strongly bonded with the metal nodes of the MOF.

To further clarify these details, as shown in figure 1(B) we were also performed the TGA of MIL-53(Al) and free BDC linkers and found that MIL-53(Al) exhibited three different weight losses. The Initial weight loss below 100 °C is attributed to the removal of weakly bonded water molecules on the surface of the MOF, while the secondary weight loss above 350 °C is attributed to the elimination of strongly bonded water molecules within the cavities of MIL-53(Al) and disintegration of the organic linkers from the MOF [22]. The third weight loss is above 500 °C and is attributed to the decomposition of the framework. However, free BDC linkers displayed only one weight loss which is associated to the complete decomposition of the organic linkers after 300 °C, respectively. These studies clearly identify the flexible nature of this MOF. Though MIL-53(Al) was primarily activated, owing to its flexible nature, it always captures the moisturizers from the environment and undergoes to the structural transitions.

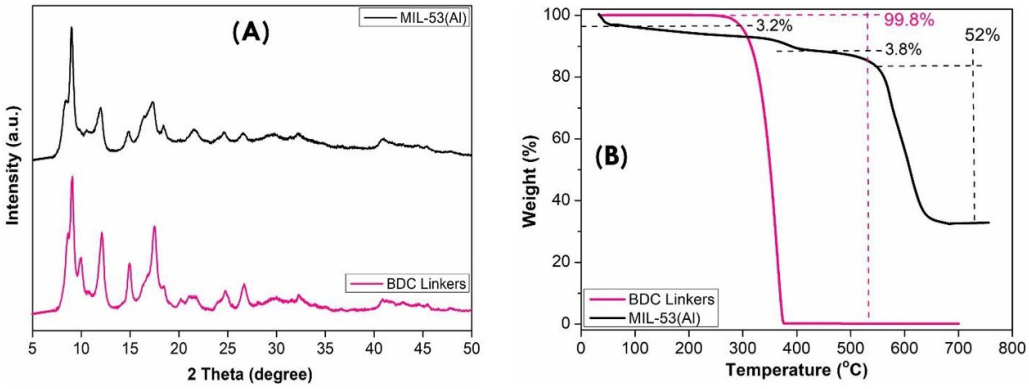

Figure 1. (A) Powder x-ray diffraction (PXRD) patterns of MIL-53(Al) and free BDC linkers. (B) Thermogravimetric (TGA) analysis of MIL-53(Al) and free BDC linkers.

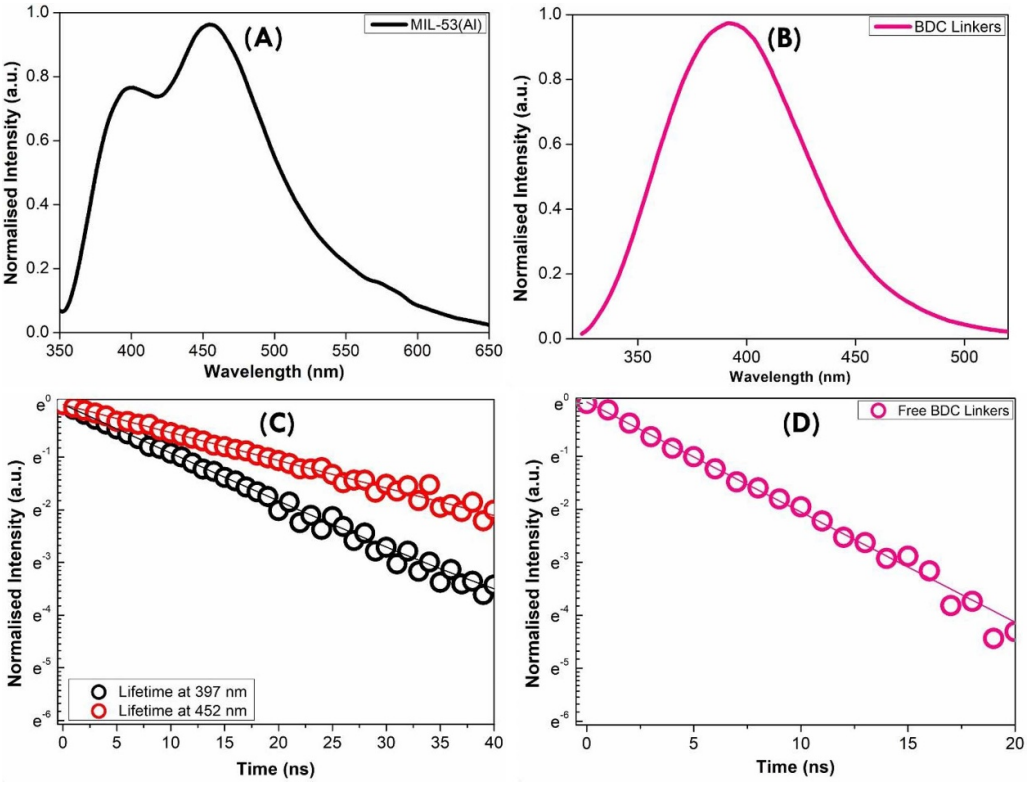

Figure 2. Photoluminescence (PL) emission spectra of MIL-53(Al) (A) and free BDC linkers (C) excited at 305 nm. Decay curves recorded at 397 nm and 452 nm in MIL-53(Al) (B) and at 388 nm in free BDC linkers (D).

3.2. PL response of MIL-53(Al) and free BDC linkers

Time-resolved PL spectra of MIL-53(Al) and free terephthalic acid (organic linker) were recorded upon UV irradiation with the excitation wavelength of $\lambda_{\text{excitation}} = 305$ nm, setting $T_{\text{W}} = 50$ ns and $T_{\text{D}} = 5$ ns. As shown in figure 2(A), MIL-53(Al) exhibits two emission bands centered at $\lambda_{\text{emission}} = 397 \pm 2$ nm nm (violet) and $\lambda_{\text{emission}} = 452 \pm 2$ nm (blue), respectively. The first band is attributed to the ligand-based charge transfer transition processes of the organic linkers, its peak position is comparable to the single emission of the free terephthalic acid (figure 2(B)), centered at $\lambda_{\text{emission}} = 388 \pm 2$ nm), that is attributed to the π–π^* transition of the benzene ring [23, 24]. As concerns the second band in MIL-53(Al), different studies associated it to the ligand to metal charge transfer (LMCT) transition mechanism [23–27].

Furthermore, time decay of the emissions in MIL-53(Al) powder and free terephthalic acid are displayed in figures 2(C) and (D), respectively. The reported curves were acquired recording to the PL intensity at the emission band, by setting the time window (T_{W}) at 1 ns while time delay (T_{D}) was increased from 0 ns in steps of 1 ns until the PL intensity was decreased down at least a factor of 10. It is observed that all the decay curves are perfectly following the single exponential laws with a lifetime that can be determined with a best fitting procedure. The lifetime associated with the first band (397 nm)

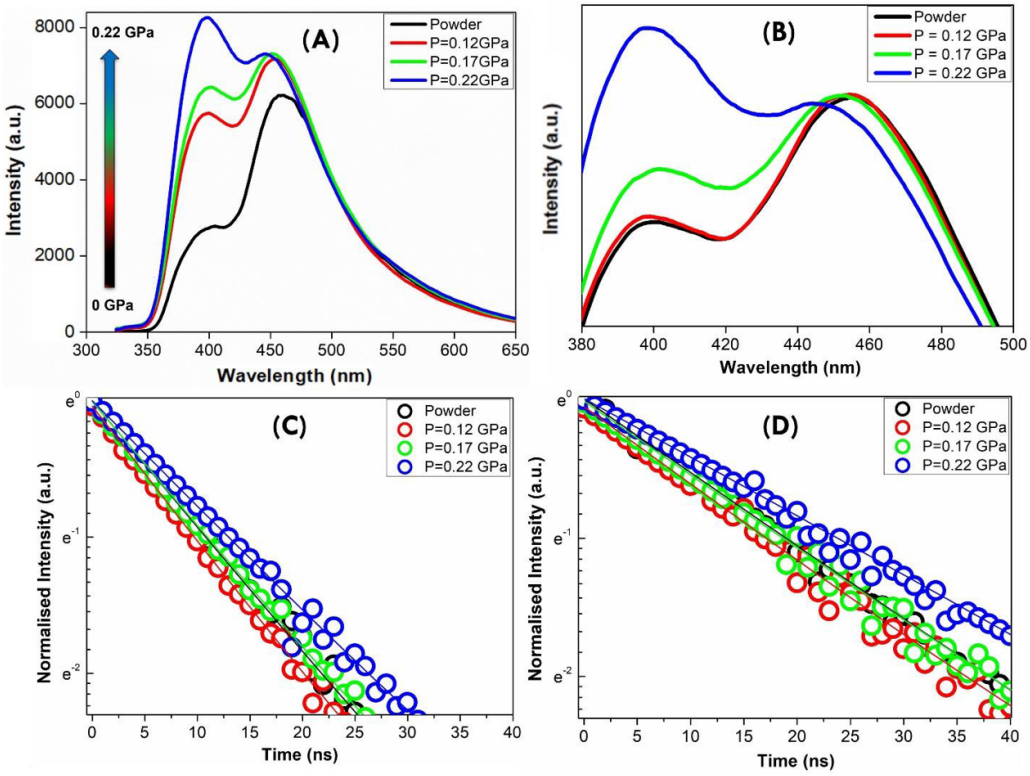

Figure 3. Photoluminescence (PL) emission spectra (A), zoomed in normalized curves (B) and decay curves recorded at 397 nm (C) and 452 nm (D) in MIL-53(Al) powder and pressed pellets with $P = 0.12$ GPa, $P = 0.17$ GPa, and $P = 0.22$ GPa, excited at 305 nm.

in MIL-53(Al) is reported as, $\tau_1 = 9.8 \pm 0.4$ ns, and we also noted that it is higher than the lifetime of the same emission in free BDC linkers, that is $\tau = 5.2 \pm 0.2$ ns. Nevertheless, it is observed that the lifetime of the second band (452 nm) in MIL-53(Al) is $\tau_2 = 15.7 \pm 0.5$ ns, respectively.

3.3. Mechanochromic response of MIL-53(Al)

For the study of pressure-induced effects, we prepared seven pellets from MIL-53(Al) MOF powder (the pressure values P being 0.044, 0.062, 0.080, 0.097, 0.12, 0.17 and 0.22 GPa) and then analyzed their PL and lifetimes properties, comparing with the powder samples. As depicted in figure 3(A), the PL intensity of both the spectra is enhancing at higher mechanical stress as compared to the powder sample. Moreover, as shown in figure 3(B), from the normalized spectra of pellets it is evidenced that at higher pressure the second emission band is about 10 ± 2 nm blue shifted as compared to the MOF powder. Similar findings have also been reported for several LMOF materials [24–28]; based on the comparison with those studies we hypothesized that the distances between the metal clusters and the organic ligands change when the MOF powder layers are subjected to a mechanical stress, which in turn affects the rotation of the benzene ring of the organic linkers [24, 28] and LMCT processes. Consequently, increased emission intensity and the spectral shift is observed.

Additionally, time decay curves recorded at 397 nm and 452 nm in MIL-53(Al) (Powder + Pellets) are displayed in figures 3(C) and (D), respectively. From these data we get the following lifetime values: for powder sample, $\tau_1 = 9.8 \pm 0.4$ ns and $\tau_2 = 15.7 \pm 0.5$ ns, for pressure $P = 0.12$ GPa, $\tau_1 = 8.9 \pm 0.4$ ns and $\tau_2 = 14.8 \pm 0.5$ ns, for $P = 0.17$ GPa, $\tau_1 = 10.1 \pm 0.4$ ns and $\tau_2 = 15.7 \pm 0.5$ ns, for $P = 0.22$ GPa, $\tau_1 = 12.6 \pm 0.4$ ns and $\tau_2 = 19.8 \pm 0.5$ ns. For further clarification, we have also presented the pressure dependent lifetimes variations in figures 4(A) and (B), respectively. These findings indicating that the mechanical pressure-induced modifications in the electronic structure of MIL-53(Al) and its interactions with organic linkers and metal nodes lead to the alterations in the PL behavior of MIL-53(Al) MOF [28]. The changes in interatomic distances and ligand-metal interactions under mechanical pressure promote radiative recombination pathways and reduce nonradiative channels, the effectiveness of the latter is well highlighted by the temperature-dependent measurements shown in paragraph 3.5. Therefore, this competition between radiative and non-radiative rates results in the observed enhancements in PL intensity and lifetimes [24, 28–30]. Overall, these findings underscore the complex relationship between pressure, and structural dynamics in modulating the PL properties of MIL-53(Al) MOF.

3.4. Vibrational spectroscopy of MIL-53(Al)

The FT-Raman spectra of MIL-53(Al) (powder + pellets) are shown in figure 5 with the most dominant vibrational spectra are appeared in the frequency range of 1590–1630 cm^{-1} and are ascribed to the asymmetric stretching vibration

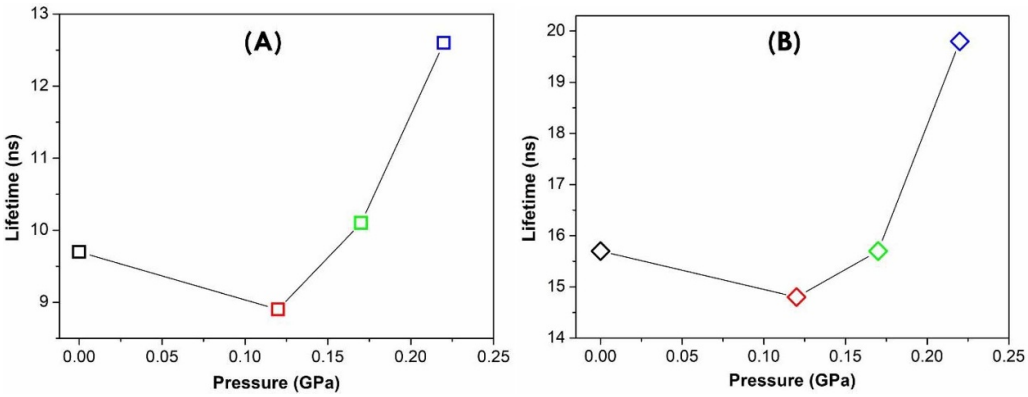

Figure 4. Lifetime values of the two emission bands centered at 397 nm (A) 452 nm (B) in MIL-53(Al) powder and pressed pellets with $P = 0.12$ GPa, $P = 0.17$ GPa, $P = 0.22$ GPa, excited at 305 nm.

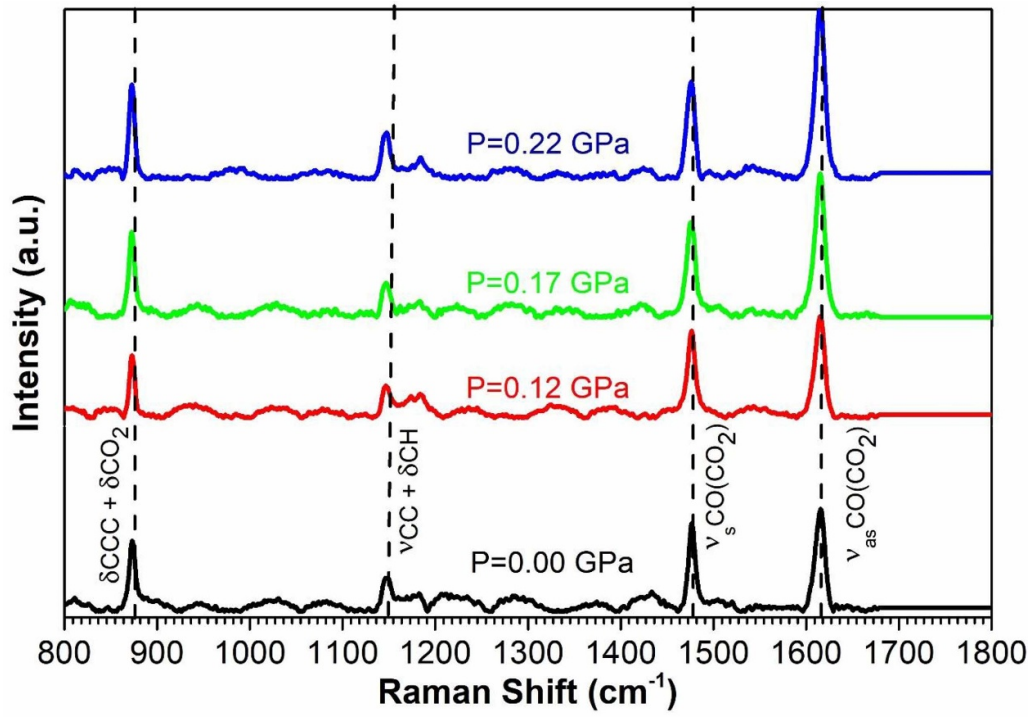

Figure 5. FT-Raman spectra of MIL-53(Al) powder and pellets with mechanical pressure ranging up to 0.22 GPa. Dotted lines indicate the positions of the main Raman peaks in the powder sample.

($\nu_{as}CO(CO_2)$) modes of the carboxylate groups of the organic linkers coordinated with the framework. The corresponding symmetric stretching vibration ($\nu_sCO(CO_2)$) modes are appearing in the frequency range of 1460–1490 cm^{-1}. Additionally, the vibrational band in the frequency range of 860–890 cm^{-1} is ascribed to the bending of aromatic ring and the bending of carboxylic group of the organic linker ($\delta CCC + \delta CO_2$). The appearance of vibrational mode in the frequency range of 1140–1150 cm^{-1} is associated with the stretching of carboxyl group and aromatic ring + H atoms rocking on the aromatic ring ($\nu CC + \delta CH$), the lines position in samples formed with different pressure is better shown in figure 6(A). Moreover, as shown in figure 6(B), there are also vibrational modes in the frequency range of 3060–3085 cm^{-1} which are likely assigned to the stretching vibration of aromatic (νCH) C–H bonds [31].

The observation of the spectra in figure 5 highlights that the greater mechanical stress induces an increase in the intensity of the Raman peaks and a slight shift to the lower energies, indicating a transition towards a more compact and closed pore configuration. After carefully analyzing our experimental data with the available literature on this material, we can hypothesize that these results are associated with the structural transitions of MIL-53(Al) MOF [31]. In this regard, we focus attention on the spectra in figures 6(A) and (B) associated with the C–H aromatic stretching vibrations and the stretching

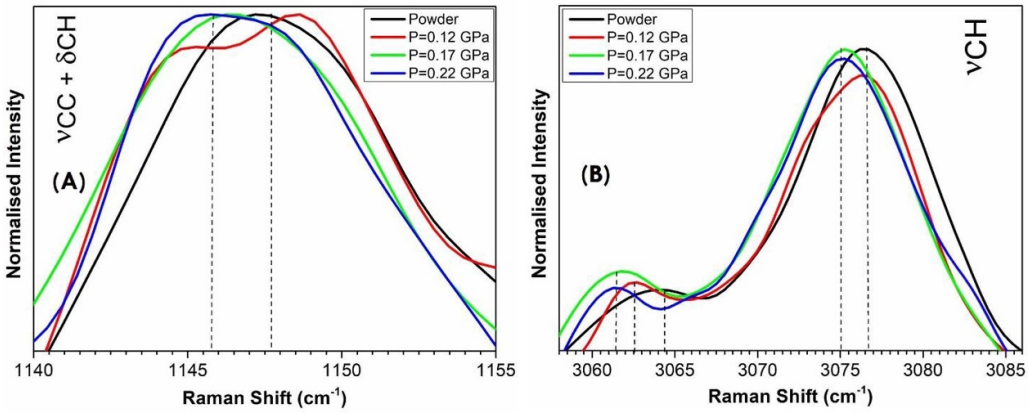

Figure 6. Normalized FT-Raman spectra of MIL-53(Al) powder and pellets with mechanical pressure ranging up to 0.22 GPa. Dotted lines indicate the positions of the main Raman peaks of the powder and pellet samples.

vibrations of the C–C and C–O bonds in the aromatic ring of the organic MOF linker. In both cases, the difference in the position of the Raman peaks between the powdered samples and the pellets ones obtained with the greater mechanical compaction of 0.22 GPa is approximately 2 cm^{-1}. These results are consistent with the alteration in the pore size and framework flexibility of MIL-53(Al) MOF due to mechanical compression, from LP to NP: the organic linker molecules are tightly arranged in the NP structure, resulting in lower-frequency vibrational modes.

3.5. Thermochromic response of MIL-53(Al) & BDC linkers

Hereafter, thermochromic PL properties are analyzed to highlight how MIL-53(Al) is sensitive to temperature changes. Therefore, emission spectra were recorded at different temperature, under excitation at 305 nm: when the sample was heated up to 400 K, the PL emission at 397 nm is partially quenched (figure 7(A)); when the sample was cooled to 300 K, the emission intensity is entirely recovered (figure 7(C)). The relative sensitivity of MIL-53(Al) in the temperature range of 320–400 K was found to be 0.5% K^{-1}. In fact, MIL-53(Al) demonstrates an edge over other materials in terms of temperature sensing due to its unique combination of structural flexibility, high surface area, and tunable pore size. These properties enable MIL-53(Al) to undergo reversible structural modifications in response to temperature variations, leading to measurable changes in PL intensity. Moreover, the proportional recovery of PL intensity with decreasing temperature makes MIL-53(Al) a prime candidate for precise and accurate temperature sensing applications.

For comparison purposes, PL temperature dependence of the free BDC linkers was also investigated on increasing (figure 7(B)) and decreasing temperature (figure 7(D)), at the same thermal cycling as in the case of MIL-53(Al) MOF. In case of BDC, the PL intensity remains approximately constant, the most notable effect being the blue-shift of about 10 nm when temperature increases from 296 K to 400 K (figure 7(H)).

Temperature-dependent lifetimes measurements of powder MIL-53(Al) and free BDC acid were also performed. As shown in figures 7(E)–(G), the decay curves are well fitted by single-exponential law, with the lifetimes in the ns range. In particular, it is observed that the lifetimes τ_1 for the band at 397 nm and τ_2 for the band at 452 nm of MIL-53(Al) decreased as the temperature increases. The reduction is particularly more evident for τ_1 which varies from 9.8 ± 0.4 ns at 300 K down to 2.5 ± 0.2 ns at 400 K, while τ_2 decreases from 15.7 ± 0.5 ns at 300 K down to 6.3 ± 0.3 ns at 400 K. In free BDC linkers, the lifetime of the band peaked around 388 nm reduces as well, from 5.2 ± 0.2 ns at 300 K to 4.4 ± 0.2 ns at 400 K.

Henceforth, the PL spectra and lifetimes measurements clearly indicated that the thermochromic response is a peculiar property of MIL-53(Al) emitting the violet band peaked at 397 nm. As shown in figure 8(B), thermal cycling effects on this emission are quite repeatable, thus meaning that it does not exhibit significant losses with each cycle (repeated five times). Therefore, MIL-53(Al) is a viable candidate as a luminous thermometer because of its capacity to reversibly detect temperature changes. According to these findings, the PL response to a thermal stimulus should be linked to structural modifications of MIL-53(Al) originating from breathing phenomena: expansion and contraction within each cycle corresponding to transitions from NP to LP and vice versa. Furthermore, several studies pointed out that ligand-based luminescence is highly dependent on the structural transitions of the framework [29, 32–34]. We hypothesized that when temperature rises, the MOF's vibrational modes likewise

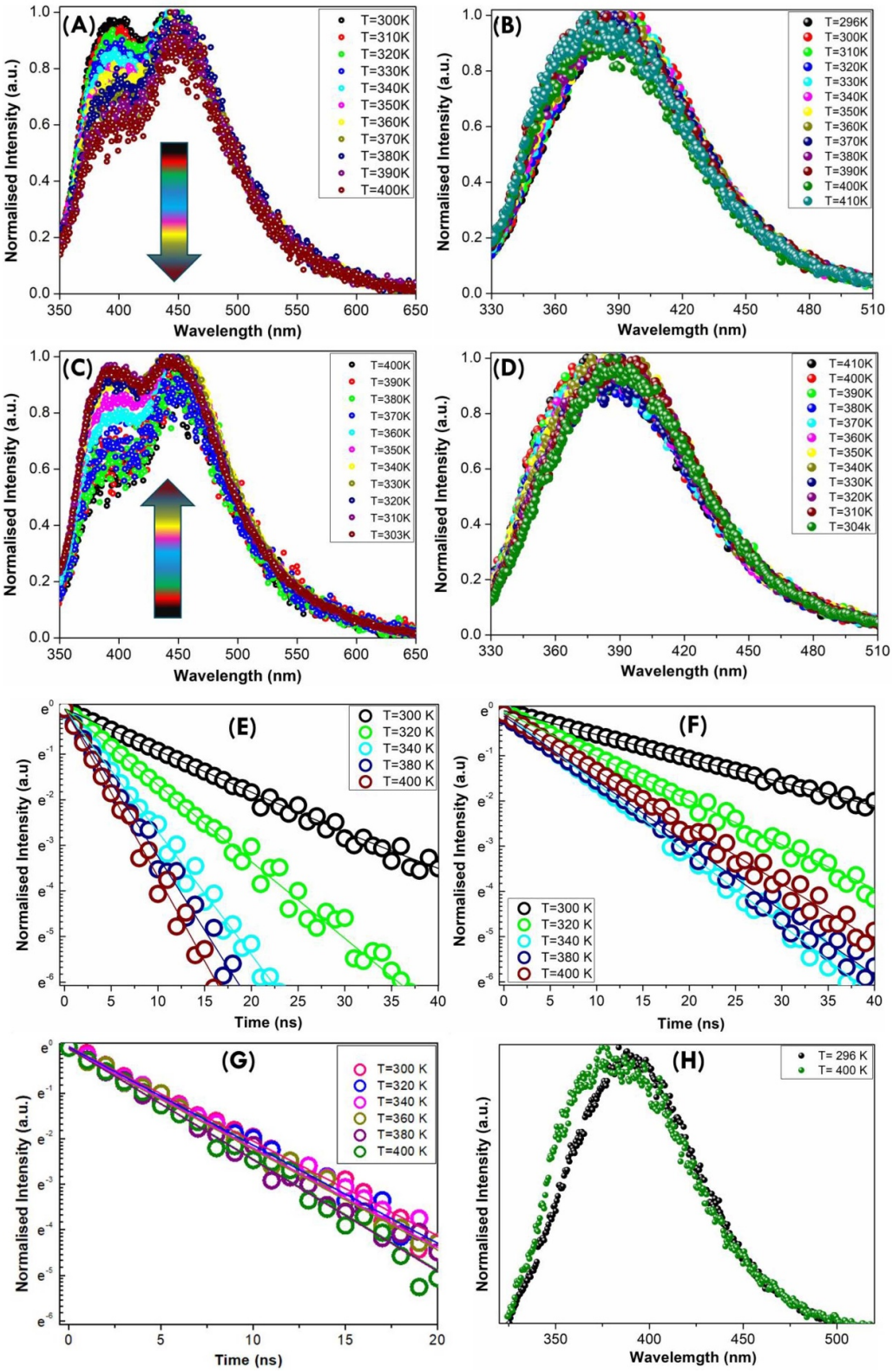

Figure 7. Temperature dependence of PL emission spectra detected under excitation at 305 nm in MIL-53(Al) (A) and free BDC linkers (B) from 300 K to 400 K, and in MIL-53(Al) (C) and free BDC linkers (D) from 400 K to 300 K. Decay curves recorded on increasing temperature from 300 K to 400 K in MIL-53(Al) at 397 nm (E) and 452 nm (F), and BDC linkers at 388 nm (G). The comparison between normalized PL spectra of free BDC linkers at 296 K and 400 K (H).

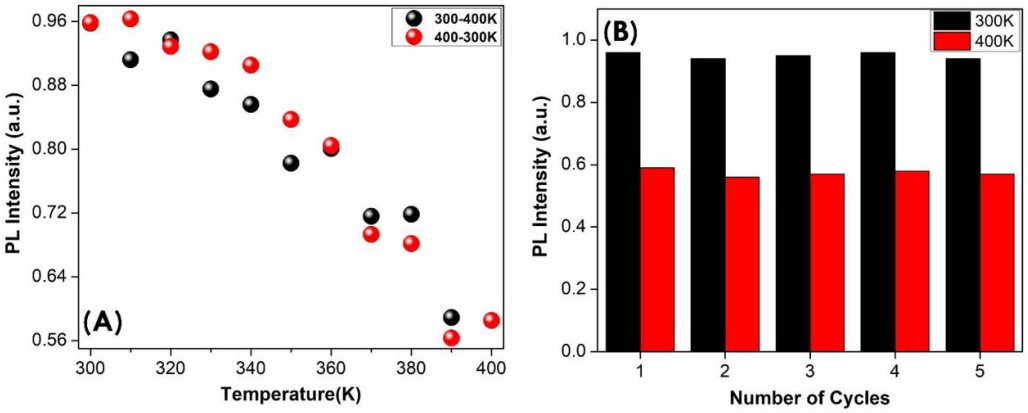

Figure 8. Photoluminescence (PL) intensity at 397 nm recorded in MIL-53(Al) during heating-cooling cycle in the range 300–400 K (A). Maximum and minimum PL intensities at 397 nm recorded in five heating-cooling cycles (B).

enlarge increasing the amount of non-radiative recombination, this causes the observed lifetime reduction.

4. Conclusions

In this work we have investigated the mechanochromic and thermochromic response of a solid-state MIL-53(Al). Under UV excitation at 305 nm, MIL-53(Al) exhibits two emission bands, both decaying in a ns timescale. The first band is centered at 397 nm and is associated with an intra-ligand charge transfer mechanism of the BDC linkers; the second is peaked at 452 nm and is related to LMCT transition. When subjected to temperature changes, MIL-53(Al) exhibits a unique Ratiometric fluorescence behavior. The emission at 397 nm is quenched when the sample is heated up to 400 K and fully recovers its value when the sample is again at room temperature. Additionally, under higher mechanical stress MIL-53(Al) displays turn-on behavior in PL emission intensity. These findings feature the sensitivity of MIL-53(Al) under mechanical compaction and hence offering interesting perspectives for the application in mechanically deformed-based luminescent sensors.

Data availability statement

All data that support the findings of this study are included within the article (and any supplementary files).

Acknowledgments

We applaud the support from University of Palermo, Department of Physics and Chemistry (DiFC).

Conflict of interest

The authors declare no conflicts of interest.

Author contributions

Conceptualization, M Cannas and G Buscarino; methodology, T Ul Rehman, M M Calvino, S Agnello and S M Gelardi; writing—original draft preparation, T Ul Rehman; writing—review and editing, M Cannas, G Buscarino, and S Agnello; supervision, M Cannas. All authors have read and unanimously agreed to the published version of the manuscript.

Funding

This research work received no external fundings.

ORCID iD

T Ul Rehman https://orcid.org/0009-0006-1024-2830

References

[1] Hafizovic J, Krivokapic A, Szeto K C, Jakobsen S, Lillerud K P, Olsbye U and Tilset M 2007 Tailoring the dimensionality of metal–organic frameworks incorporating Pt and Pd. from molecular complexes to 3D networks *Cryst. Growth Des.* **7** 2302–4

[2] Sapianik A A, Kiskin M A, Kovalenko K A, Samsonenko D G, Dybtsev D N, Audebrand N, Sun Y and Fedin V P 2019 Rational synthesis and dimensionality tuning of MOFs from preorganized heterometallic molecular complexes *Dalton Trans.* **48** 3676–86

[3] Walekar L, Dutta T, Kumar P, Ok Y S, Pawar S, Deep A and Kim K H 2017 Functionalized fluorescent nanomaterials for sensing pollutants in the environment: a critical review *TRAC-Trend Anal. Chem.* **97** 458

[4] Zhang Y, Yuan S, Day G, Wang X, Yang X and Zhou H C 2018 Luminescent sensors based on metal-organic frameworks *Coord. Chem. Rev.* **354** 28

[5] Brites C D S, Balabhadra S and Carlos L D 2019 Lanthanide-based thermometers: at the cutting-edge of luminescence thermometry *Adv. Opt. Mater.* **7** 1801239

[6] Chaudhari A K and Tan J C 2018 Mechanochromic MOF nanoplates: spatial molecular isolation of light-emitting guests in a sodalite framework structure *Nanoscale* **10** 3953

[7] Burtch N C, Heinen J, Bennett T D, Dubbeldam D and Allendorf M D 2018 Mechanical properties in metal–organic frameworks: emerging opportunities and challenges for device functionality and technological applications *Adv. Mater.* **30** 1704124

[8] Yan Y, He T, Zhao B, Qi K, Liu H and Xia B Y 2018 Metal/covalent–organic frameworks-based electrocatalysts for water splitting *J. Mater. Chem.* A **6** 15905

[9] Leng X, Zeng J, Yang M, Li C, Vattikuti S P, Chen J, Li S, Shim J, Guo T and Ko T J 2023 Bimetallic Ni–Co MOF@ PAN modified electrospun separator enhances high-performance lithium–sulfur batteries *J. Energy Chem.* **82** 484–96

[10] Zeng J, Devarayapalli K C, Vattikuti S P and Shim J 2022 Split-cell symmetric supercapacitor performance of bimetallic MOFs yolk-shell hierarchical microstructure *Mater. Lett.* **309** 131305

[11] Cui Y, Zhu F, Chen B and Qian G 2015 Metal–organic frameworks for luminescence thermometry *Chem. Commun.* **51** 7420

[12] Lustig W P, Mukherjee S, Rudd N D, Desai A V, Li J and Ghosh S K 2017 Metal–organic frameworks, functional luminescent and photonic materials for sensing applications *Chem. Soc. Rev.* **46** 3242

[13] Zhang Z, Sang W, Xie L and Dai Y 2019 Metal-organic frameworks for multimodal bioimaging and synergistic cancer chemotherapy *Coord. Chem. Rev.* **399** 213022

[14] Yang C X, Ren H B and Yan X P 2013 Fluorescent metal–organic framework MIL-53(Al) for highly selective and sensitive detection of Fe^{3+} in aqueous solution *Anal. Chem.* **85** 7441–6

[15] Xu H, Gao J, Qian X, Wang J, He H, Cui Y, Yang Y, Wang Z and Qian G 2016 Metal–organic framework nanosheets for fast-response and highly sensitive luminescent sensing of Fe^{3+} *J. Mater. Chem.* A **4** 10900

[16] Zheng J P, Ou S, Zhao M and Wu C D 2016 A highly sensitive luminescent dye@MOF composite for probing different volatile organic compounds *Chem. Plus Chem.* **81** 758

[17] Chaudhari A K, Kim H J, Han I and Tan J C 2017 Optochemically responsive 2D nanosheets of a 3D metal–organic framework material *Adv. Mater.* **29** 1701463

[18] Zhang Y, Gutiérrez M, Chaudhari A K and Tan J C 2020 Dye-encapsulated zeolitic imidazolate framework (ZIF-71) for fluorochromic sensing of pressure, temperature, and volatile solvents *ACS Appl. Mater. Interfaces* **12** 37477

[19] Rocha J, Brites C D S and Carlos L D 2016 Lanthanide organic framework luminescent thermometers *Chem. Eur. J.* **22** 14782

[20] Marciniak L, Bednarkiewicz A, Kowalska D and Strek W 2016 A new generation of highly sensitive luminescent thermometers operating in the optical window of biological tissues *J. Mater. Chem.* C **4** 5559

[21] Camarda P *et al* 2020 Synthesis of multi-color luminescent ZnO nanoparticles by ultra-short pulsed laser ablation *Appl. Surf. Sci.* **506** 144954

[22] Mishra P, Uppara H P, Mandal B and Gumma S 2014 Adsorption and separation of carbon dioxide using MIL-53 (Al) metal-organic framework *Ind. Eng. Chem. Res.* **53** 19747–53

[23] An Y, Li H, Liu Y, Huang B, Sun Q, Dai Y, Qin X and Zhang X 2016 Photoelectrical, photophysical and photocatalytic properties of Al based MOFs: MIL-53(Al) and MIL-53-NH_2(Al) *J. Solid State Chem.* **233** 194–8

[24] Xiao J, Wu Y, Li M, Liu B-Y, Huang X-C and Li D 2013 Crystalline structural intermediates of a breathing metal–organic framework that functions as a luminescent sensor and gas reservoir *Chem. Eur. J.* **19** 1891–5

[25] Zhao D, Yu S, Jiang W-J, Cai Z-H, Li D-L, Liu Y-L and Chen Z-Z 2022 Recent progress in metal-organic framework based fluorescent sensors for hazardous materials detection *Molecules* **27** 2226

[26] Liu Y Y, Ma J C, Zhang L P and Ma J F 2008 Four silver-containing coordination polymers based on bis(imidazole) ligands *J. Coord. Chem.* **61** 3583

[27] Zhuang Z and Liu D 2020 Conductive MOFs with photophysical properties: applications and thin-film fabrication *Nano-Micro. Lett.* **12** 132

[28] Li Z, Jiang F, Yu M, Li S, Chen L and Hong M 2022 Achieving gas pressure-dependent luminescence from an AIEgen-based metal-organic framework *Nat. Commun.* **13** 2142

[29] Chen C-X, Wei Z-W, Cao C-C, Yin S-Y, Qiu Q-F, Zhu N-X, Xiong Y-Y, Ji-Jun Jiang M P and Su C-Y 2019 All roads lead to rome: tuning the luminescence of a breathing catenated Zr-MOF by programmable multiplexing pathways *Chem. Mater.* **31** 5550–7

[30] Gutierrez M, Martín C, Souza B, Vder Auweraer M, Hofkens J and Tan J-C 2020 Highly luminescent silver-based MOFs: scalable eco-friendly synthesis paving the way for photonics sensors and electroluminescent devices *Appl. Mater. Today* **21** 100817

[31] Hoffman A E J, Vanduyfhuys L, Nevjestic I, Wieme J, Rogge S M J, Depauw H, Van Der Voort P, Vrielinck H and Van Speybroeck V 2018 Elucidating the vibrational fingerprint of the flexible metal–organic framework MIL-53(Al) using a combined experimental/computational approach *J. Phys. Chem.* **122** 2734–46

[32] Alhamami M, Doan H and Cheng C-H 2014 A review on breathing behaviors of metal-organic-frameworks (MOFs) for gas adsorption *Materials* **7** 3198–250

[33] Allendorf M D, Bauer C A, Bhaktaa R K and Houka R J T 2009 Luminescent metal–organic frameworks *Chem. Soc. Rev.* **38** 1330–52

[34] Zhao P, Tsang S E and Fairen-Jimenez D 2021 Structural heterogeneity and dynamics in flexible metal-organic frameworks *Cell Rep. Phys. Sci.* **2** 100544